Supporting Information

Protonic and electronic transport in hydrated thin films of the pigment eumelanin

J. Wünsche, Y. Deng, P. Kumar, E. Di Mauro, E. Josberger, J. Sayago,

A. Pezzella, F. Soavi, F. Cicoira, M. Rolandi, and C. Santato

Thermogravimetric analysis

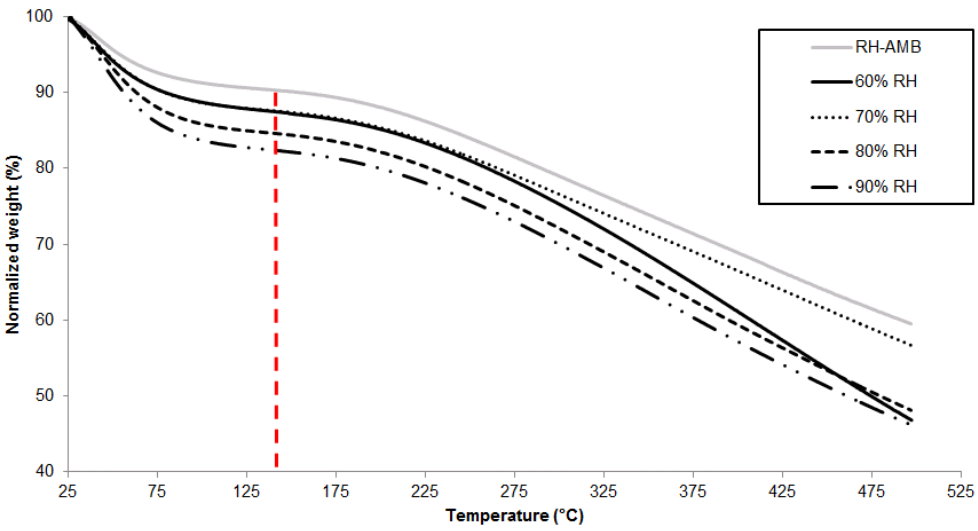

Figure S1: Thermogravimetric analysis of eumelanin powder samples hydrated at 60% to 90% RH during one day as well as a sample kept at ambient RH. The samples were heated under N_2 at a rate of 10 °C min^{-1}. The weight loss up to 140 °C is attributed to water evaporation and is given in Table S1.

Table S1: Average water content of eumelanin powder samples hydrated at different RH. The water content has been derived from the weight loss up to 140 °C as measured by thermogravimetric analysis (Figure S1). Three samples have been analyzed for each RH value.

RH	Average water content (wt%)	Standard deviation (wt%)
Ambient	8.5	1.7
60%	11.6	1.0
70%	11.9	0.5
80%	15.6	0.2
90%	16.8	0.7

Electrochemical impedance spectroscopy

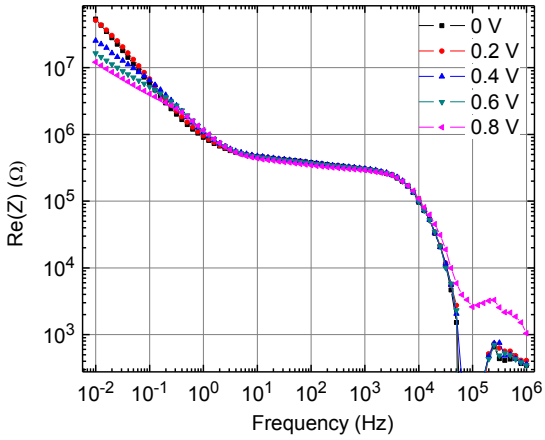

Figure S2: Frequency dependence of Re(Z) for the EIS measurement on a eumelanin film at 90% RH reported in Figure 1 of the article. A bias between 0 and 0.8 V has been applied. Sample dimensions are $L = 10$ μm, $W = 24.5$ mm, $A = 0.8$ mm^2, and $d = 50$ nm.

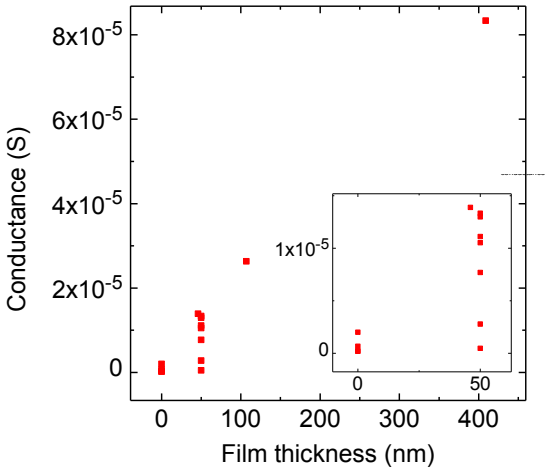

Figure S3: Ionic conductance of eumelanin thin film samples of different thickness at 90% RH, as deduced from EIS measurements. Reference measurements on bare SiO_2 substrate samples are plotted at 0 thickness. Measurements were conducted using Pt electrodes with $L = 10$ μm, $W = 24.5$ mm, $A = 0.8$ mm^2. The inset is a zoom to the data points of bare substrate and eumelanin film samples of low thickness.

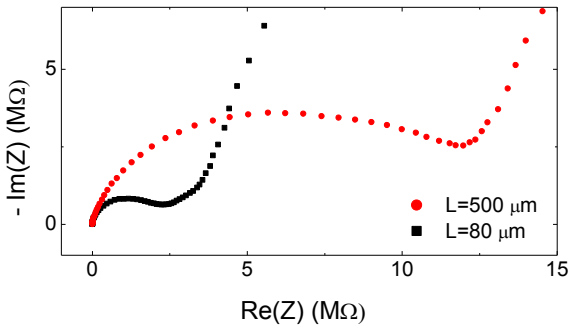

Figure S4: Nyquist plots of EIS measurement on 50 nm thick eumelanin films at 90% RH and zero bias for two different electrode distances L, 80 μm and 500 μm ($W =$ 7 mm). The diameter of the semicircles corresponds to an ionic conductivity of 1.2 and $1.5 \cdot 10^{-3}$ S cm^{-1}, respectively.

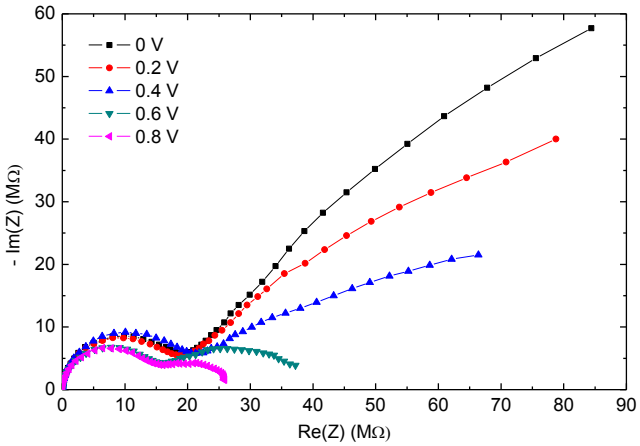

Figure S5: Nyquist plots of the EIS measurement on a eumelanin film at 90% RH, applying a bias between 0 and 0.8 V ($L = 10$ μm, $W = 4$ mm, $A = 8$ mm^2, $d = 50$ nm). The frequency range is $10^{-2} - 10^6$ Hz. The electrode geometry used in this measurement is characterized by a larger electrode area but a smaller electrode width compared to the interdigitated electrode design used in most measurements ($W = 24.5$ mm, $A = 0.8$ mm^2), including the EIS results reported in Figure 1 of the main text.

Current-voltage measurements

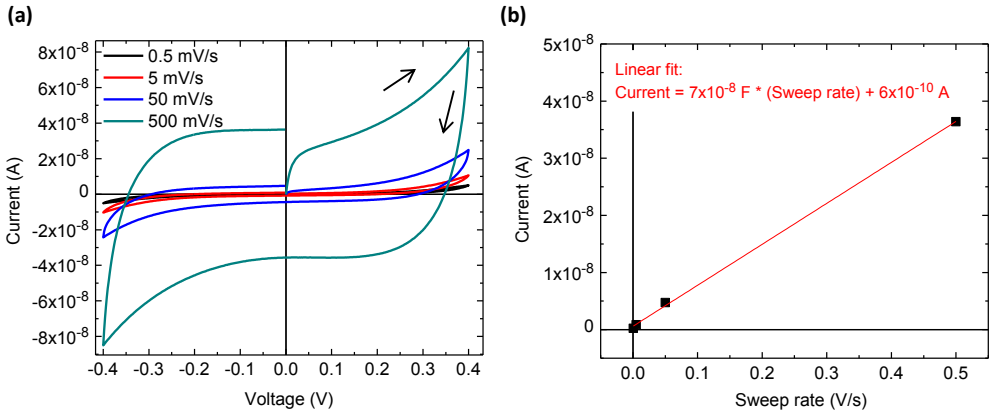

Figure S6: (a) Sweep rate-dependent current-voltage characteristics of a eumelanin film at 90% RH for [-0.4 V, 0.4 V], measured with coplanar Pt electrodes ($L = 10$ μm, $W = 24.5$ mm, $d = 50$ nm). (b) $I(0\text{ V})$ (taken at the end of the cycle) vs sweep rate. The red line is a linear fit. The slope of the fit is an estimate of the capacitance C of the sample. C divided by the in-plane electrode area (0.8 mm^2) yields 9 μF cm^{-2}.

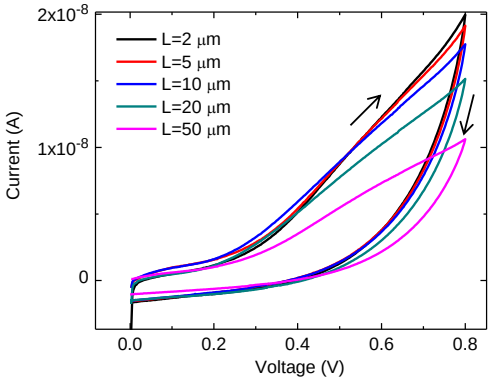

Figure S7: Current-voltage characteristics of eumelanin films at 90% RH for different electrode spacings L ($W = 1.5$ mm, $d = 30$ nm). The sweep rate is 5 mV s^{-1}. $I(0.8\text{ V})$ increases when L decreases from 50 μm to 10 μm, indicating that the current is partly limited by (mass or charge) transport in the bulk. $I(0.8\text{ V})$ saturates at $L = 2$ μm to 5 μm. This suggests that the current is limited by charge transfer at the electrodes for relatively low values of L.

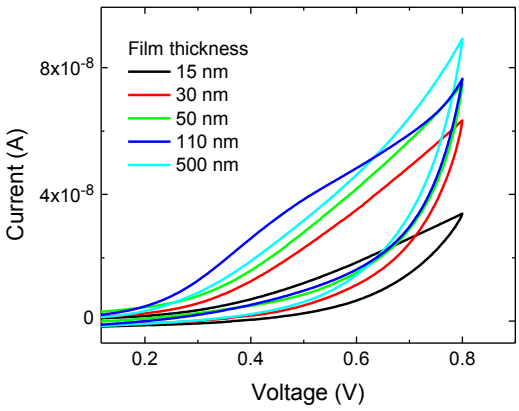

Figure S8: Current-voltage characteristics (sweep rate 5 mV s^{-1}) of eumelanin films of different thickness at 90% RH ($L = 10$ μm, $W = 24.5$ mm). $I(0.8\text{ V})$ scales with the film thickness only up to 30 nm, indicating that at higher film thickness the current is limited by interface processes rather than by transport in the bulk.

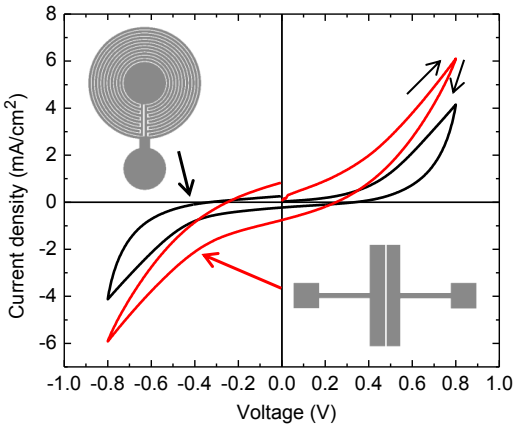

Figure S9: Current density-voltage characteristics (sweep rate 5 mV s^{-1}) of eumelanin films ($d = 50$ nm) at 90% RH using two different electrode geometries shown in the insets (both $L = 10$ μm). The electrode width and in-plane area is 4 mm and 8 mm^2 for the geometry with straight electrodes (red curve) and 24.5 mm and 0.8 mm^2 for the circular interdigitated design (black curve). The dependence of the current density, as evaluated taking into account only the film cross section ($W \cdot d$), on the in-plane area A suggests the contribution of electrochemical reactions to the current.

Cyclic voltammetry

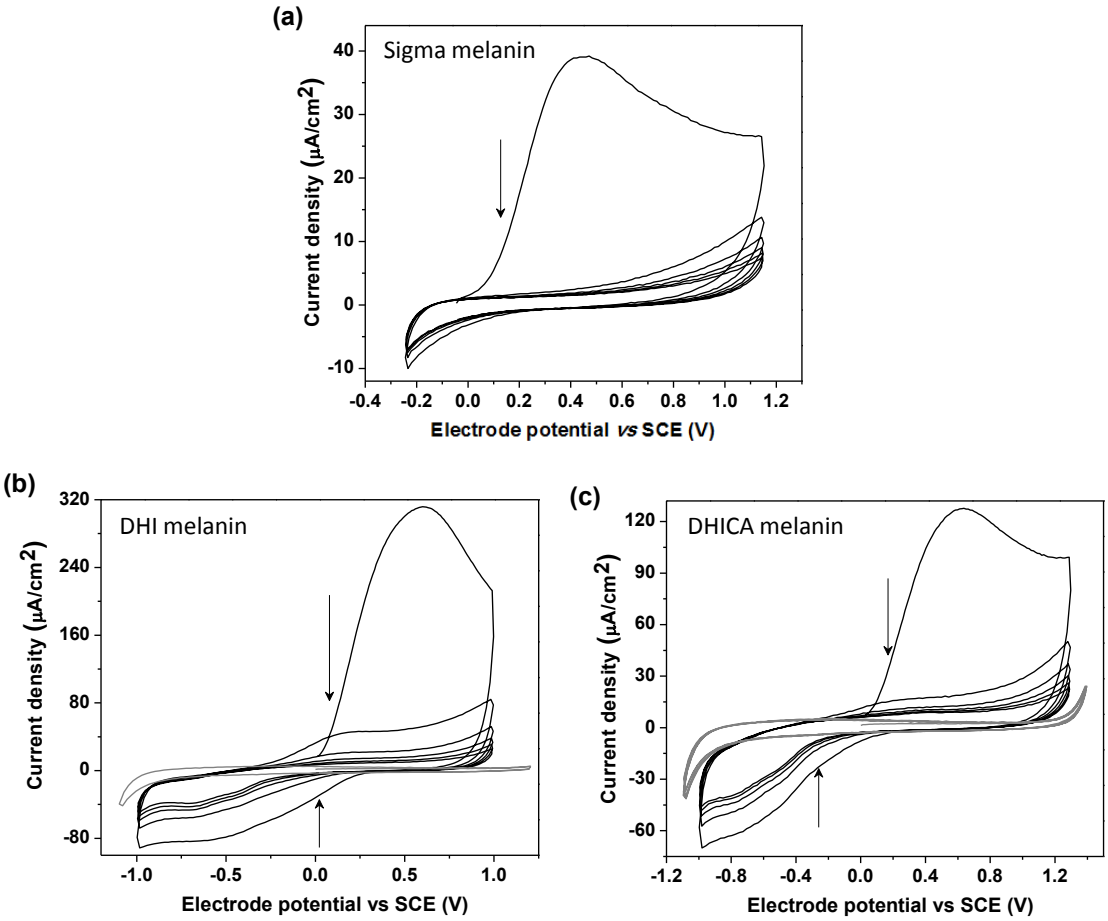

Figure S10: Cyclic voltammetry of *Sigma melanin* (a), *DHI melanin* (b), and *DHICA melanin* films (c) on ITO substrates as working electrode, platinum foil and saturated calomel electrode as the counter and the reference electrodes, respectively. Nitrogen purged PBS buffer (0.01 M) of pH 7.4 is used as the electrolyte and a 50 mV s^{-1} scan rate is maintained. The voltage is cycled from 0 to positive V and then to negative. The cyclic voltammogram of ITO without melanin in PBS is represented in gray. Black arrows indicate the decrease in current density as a function of the number of cycles.

X-ray photoelectron spectroscopy

The elemental composition of *Sigma melanin* films deposited from DMSO as obtained by a XPS wide-scan survey is given in Table S2. High-resolution spectra of the C1s, N1s, and O1s core levels are displayed in Figure S12. Binding energies and identification of the components used for peak fitting can be found in TableS3. The peak fitting and the analysis of the data regarding the monomer composition of *Sigma melanin* was guided by the standard oxidative pathway for eumelanin from tyrosine (Figure S11). We also included the possibility that pyrrolic acids form due to oxidative degradation, as well as that they can be incorporated in the macromolecular structure [1] (see end of SI). Thus, we considered the possible presence of the species A-G as given in Figure S11. To estimate the relative contribution of these units to *Sigma melanin*, we solved a system of equations based on the theoretical (for the monomers) and experimental (for *Sigma melanin*) values of the elemental ratios [C]/[N], [O]/[N], the portion of C bound in carboxyl groups, and the portion of N in pyrrole rings vs. uncyclized structures (Table S4). These quantities were judged the most reliable from the XPS spectra and the most useful to distinguish the species A-G. Based on our assumptions, the values given in Table S4 do not allow a significant content of pyrrolic acids, E-G. Indeed, we obtain a composition of 22% DHI units, 41% DHICA units, 37% of L-dopa or tyrosine based on [C]/[N], [C in COOH], and [N in pyrrole]. This composition corresponds to [O]/[N]=3.6, which is lower than the measured ratio but within the experimental error, considering also the presence of impurities. The result can change if other N-containing uncyclized molecules or hydrocarbon contamination are taken into account. Further structural characterization is required to obtain a complete picture of the chemical composition of *Sigma melanin*.

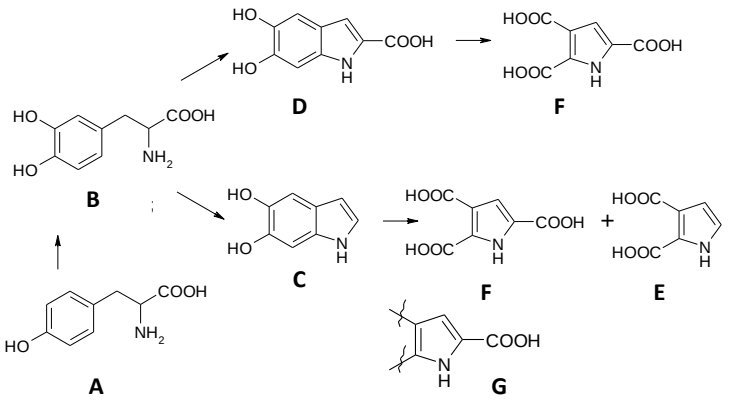

Figure S11: Standard oxidative pathway for the formation of eumelanin from tyrosine (A), via L-dopa (B), DHI (C), and DHICA (D). DHI and DHICA polymerized to give eumelanin. Pyrrole-2,3-dicarboxylic acid (E) and pyrrole-2,3,5-tricarboxylic acid (F) are the main oxidative degradation products of eumelanin and can also be incorporated into the macromolecular structure in the form of specie G.

Table S2: XPS wide scan survey results for a thin film of commercial synthetic eumelanin deposited from dimethyl sulfoxide.

	Binding energy (eV)	Atomic %
Pt4f	74.1	0.1
S2p	167.1	0.4
Cl2p	198.7	0.1
C1s	285.1	61.9
N1s	399.8	7.0
O1s	531.9	27.9
F1s	688.0	2.0
Fe2p3	708.9	0.6

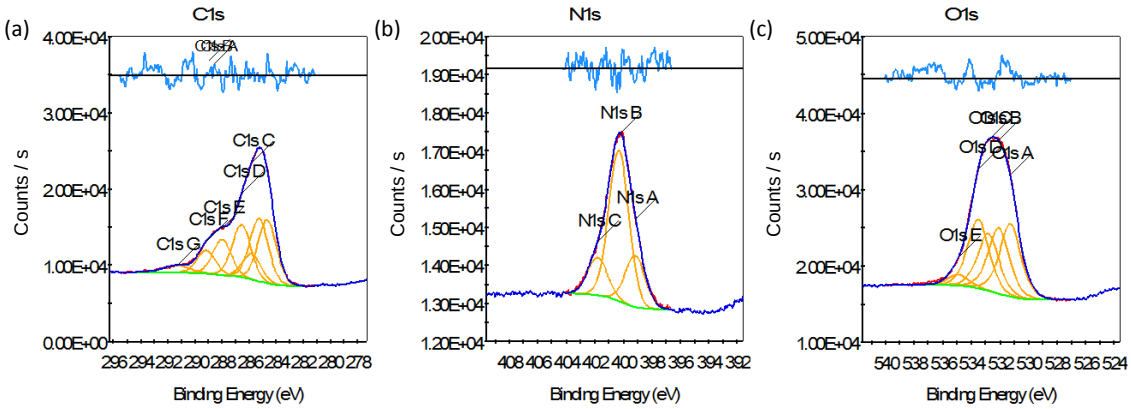

Figure S12: XPS spectra of a eumelanin thin film. C1s (a), N1s (b), and O1s core level (c). The assignment of the individual components used for peak fitting can be found in Table S3.

Table S3: Chemical moieties used to fit the XPS spectra of a eumelanin thin film. The composition is normalized to 100 % for each element. The systematic error in the high-resolution XPS analysis of chemically heterogeneous materials such as eumelanin is typically 10% in relative terms.

Element	Binding energy (eV)	Assignment	Atomic %
C	284.7	C-C aromatic	23.1
	285.3	C-C aromatic	23.0
	285.8	-C-N	9.3
	286.5	-C-OH, -C-N	19.3
	288.0	-C=O	13.0
	289.2	O=C-OH	8.5
	291.4	$\pi - \pi^*$ in C=C	3.9
N	399.2	$-NH_2$	21.4
	400.3	pyrrole	62.9
	401.8	$-NH_3^+$	15.7
O	531.3	O=C	27.5
	532.1	O=C in COOH	24.7
	532.8	HO-C in COOH	21.7
	533.5	HO-C aromatic	26.1

Table S4: The theoretical (for species A-G) and experimental (for *Sigma melanin*) values of the elemental ratios [C]/[N], [O]/[N], the portion of C bound in carboxyl groups, and the portion of N in pyrrole rings.

		[C]/[N]	[O]/[N]	[C in COOH]/[C_{total}]	[N cyclized]/[N_{total}]
A	Tyrosine	9	3	0.11	0
B	L-dopa	9	4	0.11	0
C	DHI	8	2	0	1
D	DHICA	9	4	0.11	1
E	Pyrrole-2,3-dicarboxylic acid	6	4	0.33	1
F	Pyrrole-2,3,5-tricarboxylic acid	7	6	0.43	1
G	Pyrrole-2,3,5-tricarboxylic acid linked	7	2	0.14	1
	Sigma melanin	8.88	4	0.085	0.63

Proton current

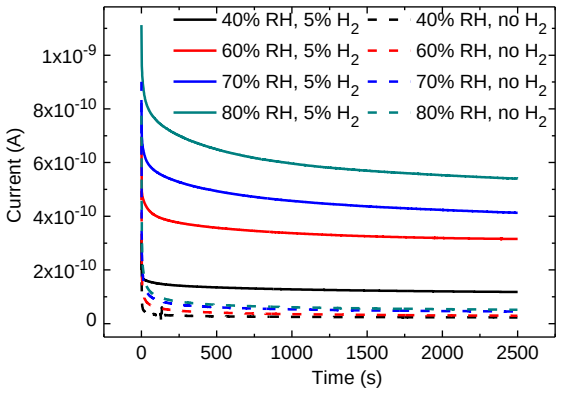

Figure S13: Transient current measurements ($V = 0.5$ V) on a drop-cast eumelanin thin film with Pd electrodes ($W = 20$ μm, $L = 6$ μm) under proton- and electron-injecting (5% H_2 in atmosphere) and only electron-injecting conditions (no H_2) for different values of relative humidity.

References

[1] A. Napolitano, A. Pezzella, G. Prota, R. Seraglia, and P. Traldi, *Rapid Commun. Mass Spectrom.*, vol. 10, no. 4, pp. 468472, 1996.